Electronic Supplementary Material (ESI) for Catalysis Science & Technology.

Supporting Information for:

Exploring CO_2 Hydrogenation to Methanol at a Cu/Zn–ZrO_2 Interface via DFT Calculations

Aku Lempelto, Lars Gell, Toni Kiljunen, and Karoliina Honkala*

Department of Chemistry, Nanoscience Center, P.O. Box 35, FI-40014, University of Jyväskylä, Finland

E-mail: karoliina.honkala@jyu.fi

We collect the structure images of the RWGS/Formate route elementary steps $\mathrm{R/F}_i \rightarrow \mathrm{TS}_j \rightarrow \mathrm{R/F}_k$ that take place on the nanorod–metal-oxide interfaces. For the sake of clarity, the oxygen atoms of the intermediates and transition states have been coloured with brighter red than the lattice oxygens. All hydrogens are white, carbon is dark grey, Zn atoms are coloured purple, Zr atoms turquoise, and Cu atoms orange.

List of Figures

List of Tables

Contents

1 Alternative intermediates and pathways

Here we discuss several alternative paths through intermediates that were calculated but that were ultimately deemed unfavourable or otherwise not relevant to the main text.

1.1 Direct dissociation of CO_2

We explored the possibility of the adsorbed CO_2 dissociating directly into CO and O as shown in Fig. S1. To facilitate this, the CO_2 was adsorbed on a location that binds it 0.61 eV less strongly than the optimal site discussed in main article. This type of geometry was chosen to avoid extensive reaction paths which are prone to convergence errors and expensive to calculate. At the Zn-rich interface, the activation energy of dissociation (TS_{22}) is $+1.12$ eV while the dissociation products together are exothermic by -0.18 eV. That is, the products are 0.43 eV uphill from the optimal CO_2 adsorption. During dissociation, the CO molecule moved from the Zn atom to the neighbouring Cu atom while the oxygen atom was left bridged between two Zn atoms and on-top of an underlying Zr atom. We note that the mechanism varied from one interface to another due to the different Cu/Zn contents and interactions with CO. Due to the high energy cost associated with the direct dissociation step, the resulting structures were disregarded for further reaction steps.

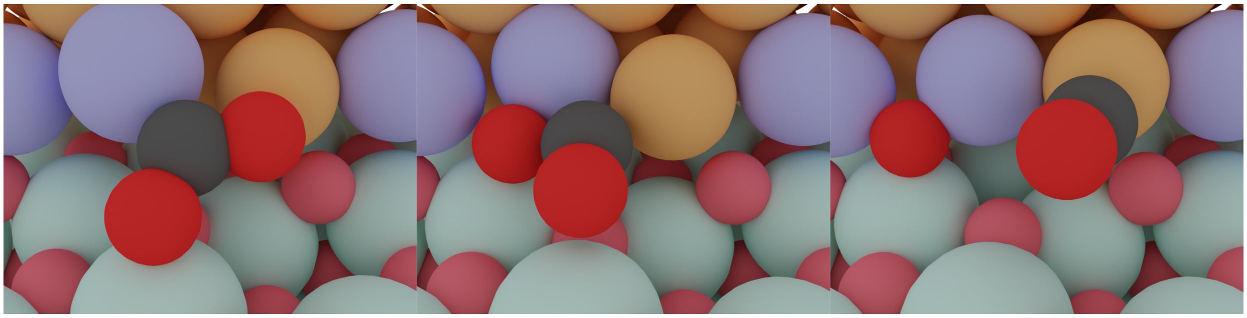

Figure S1: CO_2 dissociation at the Zn-rich interface. Light red: lattice O, dark red: adsorbate O, dark grey: C, purple: Zn, turquoise: Zr, orange: Cu.

1.2 Formic acid

Previous studies have reported that the formation of HCOOH from formate (HCOO) has an activation energy around 0.8–0.9 eV.[1–4] On this basis, it was suggested to be the preferable pathway forward from HCOO on Cu surface models and some cluster models. Therefore we also considered the reaction on CuZn/ZrO_2. The H atom preferably transfers from a surface oxygen to reach the oxygen atom of the intermediate, which tends to lower the activation energy as compared to the feed of a H atom from the metal. If formed, the HCOOH can further hydrogenate into a type of hydroxymethoxy species H_2COOH. This reaction is exothermic by -0.7 eV to -0.9 eV with an activation energy of 0.4 eV at the Zn-dilute interface, which is comparable to the previously reported values.

Similarly, a potentially competing process to breaking the C–O bond in COOH is its hydrogenation to HCOOH. While this reaction is more exothermic than the splitting at all the interfaces, we were unable to find a proper transition state. Instead, the calculations led to a spontaneous cleavage of the C–O bond, yielding HCO and an OH. Therefore we assume the dominant mechanism to go via HCO formation.

1.3 Hydroxymethyl path

In the alternative pathway forward from formaldehyde (H_2CO), the H atom transfers from a lattice oxygen to form hydroxymethyl (H_2COH). The reaction is nearly isoenergetic and independent of the presence of OH on the surface. The activation energies with and without OH are ~ 0.1 eV (TS_{17}) and 0.1–0.6 eV (TS_{08}), respectively. For comparison, the Cu(111) surface[1] shows similar reaction energies (-0.06 eV) with slightly higher values for the activation energy (0.82 eV). H_2COH can also be produced from HCOH but this pathway has large kinetic barriers, ranging between 0.8 eV and 1.5 eV for the Zn-dilute and Zn-rich interface, respectively (see table S2). This barrier is substantially higher than the 0.46 eV value previously obtained on a Cu(111) surface.[1] This could simply be due to the HCOH binding at the CuZn interface having a less favourable geometry than the same intermediate binding to Cu(111) via its carbon. The ease of deformation of the Zn–containing interfaces means that the Zn gets pulled out significantly by the HCOH attached to it.

To complete the cycle, the H_2COH can be hydrogenated to H_3COH. In this case the H atom is again transferred from the metal component at the interface. This reaction is highly exothermic by -1.3 eV with an OH nearby and -1.0 eV without one. The activation energy also depends on the presence of a nearby OH as well as the interface type. Without OH, the barrier is ~ 1.5 eV (TS_{10}) at all interfaces. However, with the OH, the barriers are 0.65 eV for the Zn-rich and 1.13 eV for the Zn-dilute interface, respectively (see TS_{20} energies in Table S2). The relatively low barrier at the Zn-rich interface is accompanied by a temporary donation of a proton from the H_2COH hydroxyl group to the neighbouring OH. After the transition state is passed, the proton transfers back to the H_2COH. This temporary hydrogen–accepting feature of the ZrO_2-bound OH affects the transition state energy. The OH also seems to have a stabilising effect on the methanol product, likely due to strong intermolecular interaction between the OH and the adsorbate hydrogens (HO–H_3COH distance ~ 3.0Å).

1.4 Methanol dissociation into CH_3

Instead of desorbing, methanol can decompose into a methyl (H_3C) and an OH species. This splitting has an activation energy of 1.4 eV (TS_{21}) which is quite close to the energy necessary to remove methanol from the surface. However, the splitting is highly endothermic at the Zn-dilute interface and only slightly exothermic at the Zn-rich interface. We therefore consider it unlikely under normal reaction conditions, although small amounts of methane are known to form.[5,6] Nevertheless, if H_3C is formed, it can be further hydrogenated to methane or combined with other hydrocarbons to form longer chains.[5]

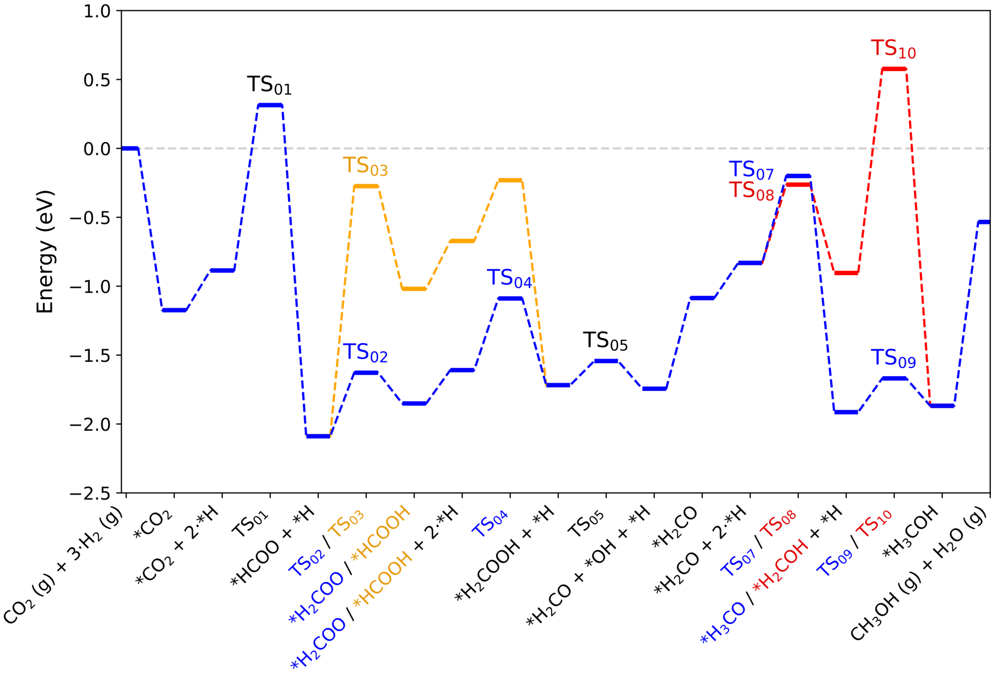

Figure S2: Energy diagram for the formate pathway on Zn-dilute interface.

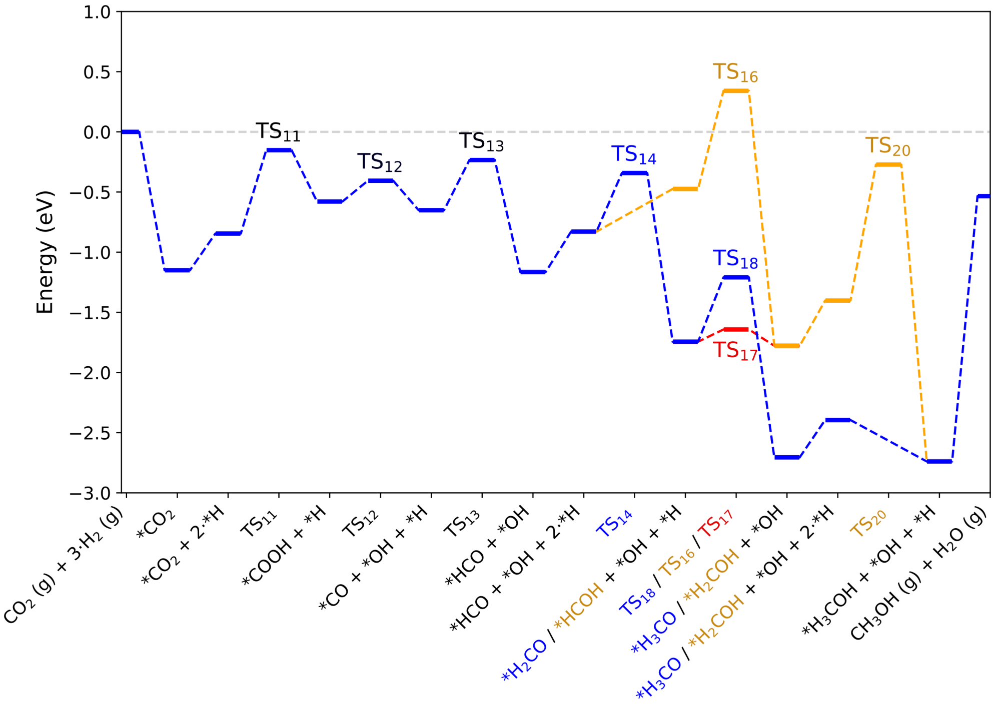

Figure S3: Energy diagram for the RWGS pathway on Zn-dilute interface.

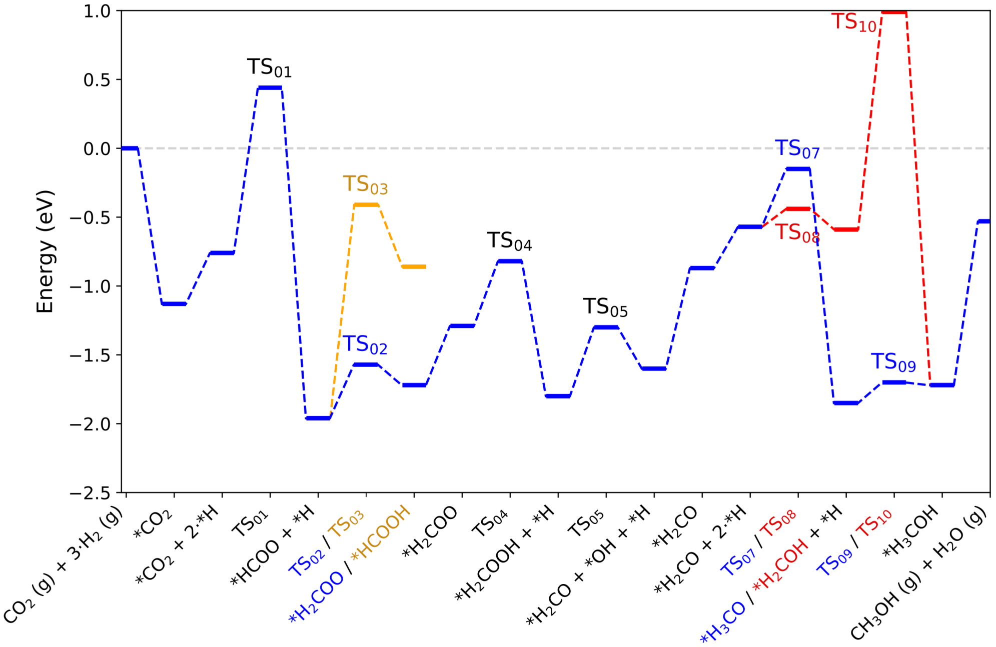

Figure S4: Energy diagram for the formate pathway on Zn-rich interface.

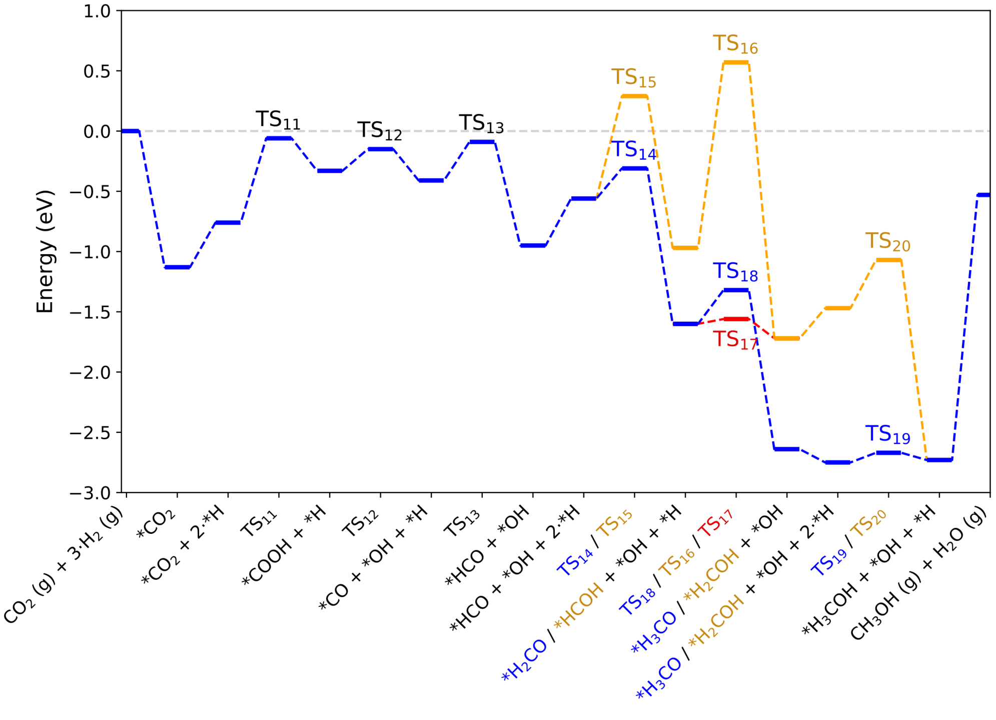

Figure S5: Energy diagram for the RWGS pathway on Zn-rich interface.

2 Energies and structures

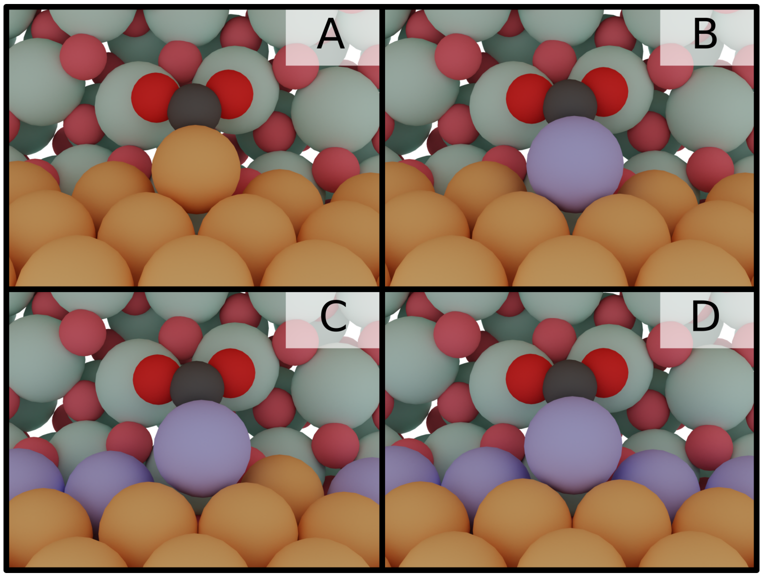

Figure S6: CO_2 adsorption geometry from a top view at all four interfaces. Light red: lattice O, dark red: adsorbate O, dark grey: C, purple: Zn, turquoise: Zr, orange: Cu.

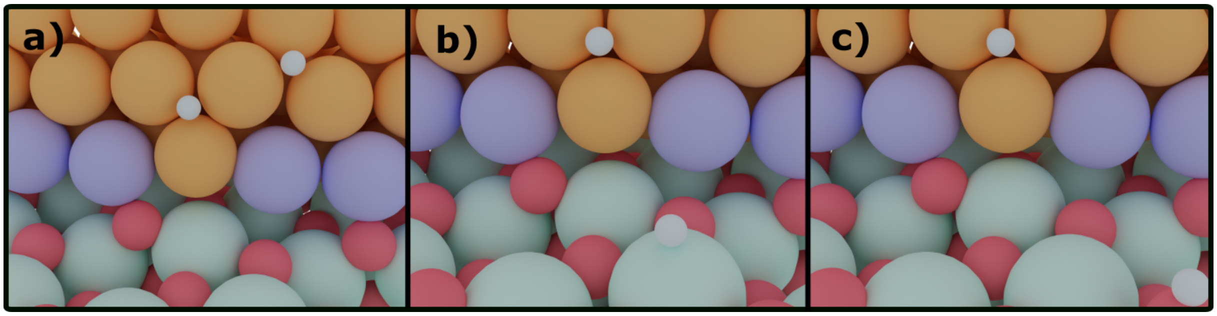

Figure S7: Different positions for adsorbed H atoms after dissociation and possible spillover (shown at the Zn-rich interface): a) both H atoms on the metal side of the interface, b) one H atom moved to a Zr, and c) one H atom moved to an O (visible in bottom right corner). Red: O, white: H, purple: Zn, turquoise: Zr, orange: Cu.

Table S1: Energy penalties of rod deformation due to CO_2 adsorption

Interface	$E_{\mathrm{CuZn/ZrO_2}}$ (eV)	$E^{*}_{\mathrm{CuZn/ZrO_2}}$ (eV)	ΔE_{def} (eV)
Cu	−12689.256	−12687.551	+1.705
Zn-dilute	−12692.499	−12691.355	+1.144
Zn	−12701.982	−12702.128	−0.146

Table S2: Energies (eV, relative to gas-phase reactants) of various intermediates (black) and transition states (red) on the four interface models. ΔE_r^* represent energies relative to the previous intermediate. The atom/part that is added or separated during a step is indicated by ‡.

Shorthand	State	Prev. intermediate	E_{ads} @Cu	ΔE_r^* @Cu	E_{ads} @Zn-dilute	ΔE_r^* @Zn-dilute	E_{ads} @Zn-rich	ΔE_r^* @Zn-rich	E_{ads} @Zn	ΔE_r^* @Zn	Location
I_{00}	$CO_2(g) + 3\ H_2(g)$	—	0.00	0.00	0.00	0.00	0.00	0.00	0.00	0.00	—
TS_{00}	$CO_2^{\ddagger}$	I_{00}	+0.38	+0.38	—	—	+0.16	+0.16	—	—	interface
I_{01}	$*CO_2$	I_{00}	−0.64	−0.64	−1.17	−1.17	−1.13	−1.13	−1.30	−1.30	interface
I_{02}	$*CO_2 + 2\cdot *H$	I_{01}	−0.76	−0.12	−0.89	+0.28	−0.76	+0.37	−0.93	+0.37	interface
TS_{01}	$*H^{\ddagger}COO + *H$	I_{02}	+0.27	+1.03	+0.31	+1.20	+0.44	+1.12	+0.24	+1.17	interface
F_{01}	$*HCOO + *H$	I_{02}	−2.10	−1.34	−2.09	−1.20	−1.96	−1.12	−2.21	−1.28	ZrO_2
TS_{02}	$*H^{\ddagger}HCOO$	F_{01}	—	—	−1.63	+0.43	-1.57	+0.39	−1.64	+0.57	ZrO_2
F_{02}	$*H_2COO$	F_{01}	−1.69	+0.41	−1.85	+0.24	−1.72	+0.23	−1.87	+0.34	ZrO_2
TS_{03}	$*HCOOH^{\ddagger}$	F_{01}	—	—	−0.27	+1.82	−0.41	+1.54	—	—	ZrO_2
F_{03}	$*HCOOH$	F_{01}	−1.03	+1.07	−1.02	+1.07	−0.86	+1.10	−0.79	+1.42	ZrO_2
F_{04}	$*H_2COO + 2\cdot *H$	F_{02}	−1.46	+0.23	−1.61	+0.24	−1.29	+0.43	−1.55	+0.32	ZrO_2
TS_{04}	$*H_2COOH^{\ddagger} + *H$	F_{04}	—	—	−1.09	+0.52	−0.82	+0.47	−0.93	+0.62	ZrO_2
F_{05}	$*H_2COOH + *H$	F_{04}	−1.72	−0.26	−1.72	−0.11	−1.80	−0.51	−1.76	−0.21	ZrO_2
TS_{05}	$*H_2CO + OH^{\ddagger} + *H$	F_{05}	—	—	−1.53	+0.19	−1.30	+0.50	—	—	interface
F_{06}	$*H_2CO + *OH + *H$	F_{05}	−1.37	+0.35	−1.74	−0.02	−1.60	+0.20	−1.83	−0.07	interface
TS_{06}	$*H_2COHOH^{\ddagger}$	F_{05}	—	—	—	—	−0.88	+0.92	—	—	ZrO_2
F_{07}	$*H_2COHOH$	F_{05}	−1.57	+0.15	−1.50	+0.22	−1.56	+0.34	—	—	ZrO_2
F_{08}	$*H_2CO$	F_{06}	−0.61	+0.76	−1.09	+0.65	−0.87	+0.74	—	—	interface
F_{09}	$*H_2CO + 2\cdot *H$	F_{08}	−0.47	+0.14	−0.83	+0.26	−0.57	+0.29	—	—	interface
TS_{07}	$*H^{\ddagger}H_2CO + *H$	F_{09}	—	—	−0.20	+0.63	−0.15	+0.43	—	—	interface
F_{10}	$*H_3CO + *H$	F_{09}	−1.93	−1.46	−1.91	−1.08	−1.85	−1.28	—	—	ZrO_2
TS_{08}	$*H_2COH^{\ddagger} + *H$	F_{09}	—	—	−0.28	+0.55	−0.44	+0.13	—	—	interface
F_{11}	$*H_2COH + *H$	F_{09}	−0.49	−0.02	−0.90	−0.07	−0.59	−0.02	—	—	interface
TS_{09}	$*H_3COH^{\ddagger}$	F_{10}	—	—	−1.67	+0.24	−1.70	+0.15	—	—	ZrO_2
TS_{10}	$*H^{\ddagger}H_2COH$	F_{11}	—	—	+0.58	+1.48	+0.99	+1.58	—	—	interface
F_{12}	$*H_3COH$	F_{10}	−1.92	+0.01	−1.87	+0.04	−1.72	+0.13	—	—	ZrO_2
TS_{11}	$*COOH^{\ddagger} + *H$	I_{02}	−0.11	+0.65	−0.17	+0.72	−0.06	+0.70	−0.18	+0.76	interface
R_{01}	$*COOH + *H$	I_{02}	−0.37	+0.39	−0.60	+0.29	−0.33	+0.42	−0.48	+0.45	interface
TS_{12}	$*CO + OH^{\ddagger} + *H$	R_{01}	—	—	−0.44	+0.16	−0.15	+0.18	−0.17	+0.31	interface
R_{02}	$*CO + *OH + *H$	R_{01}	−0.76	−0.39	−0.65	−0.05	−0.41	−0.08	−0.63	−0.15	interface
TS_{13}	$*H^{\ddagger}CO + *OH$	R_{02}	—	—	−0.23	+0.56	−0.09	+0.32	+0.04	+0.67	interface
R_{03}	$*HCO + *OH$	R_{02}	−0.77	−0.01	−1.17	−0.38	−0.95	−0.54	−1.05	−0.42	interface
R_{04}	$*HCO + *OH + 2\cdot *H$	R_{03}	−0.69	+0.08	−0.83	+0.34	−0.56	+0.39	−0.60	+0.45	interface
TS_{14}	$*H^{\ddagger}HCO + *OH + *H$	R_{04}	—	—	−0.34	+0.49	−0.31	+0.25	−0.07	+0.53	interface
R_{05}	$*H_2CO + *OH + *H$	R_{04}	−1.37	−0.68	−1.74	−0.91	−1.60	−1.04	−1.83	−1.23	interface
TS_{15}	$*HCOH^{\ddagger} + *OH + *H$	R_{04}	—	—	—	—	+0.29	+0.85	+0.34	+0.94	interface
R_{06}	$*HCOH + *OH + *H$	R_{04}	−0.35	+0.34	−0.47	+0.36	−0.97	−0.40	−1.02	−0.42	interface
TS_{16}	$*H^{\ddagger}HCOH + *OH$	R_{06}	—	—	+0.34	+0.81	+0.57	+1.53	—	—	interface
TS_{17}	$*H_2COH^{\ddagger} + *OH$	R_{05}	—	—	−1.64	+0.10	−1.56	+0.04	—	—	interface
R_{07}	$*H_2COH + *OH$	R_{05}	−1.32	+0.05	−1.78	−0.04	−1.72	−0.11	—	—	interface
R_{08}	$*H_2COH + *OH + 2\cdot *H$	R_{07}	−0.95	+0.37	−1.40	+0.38	−1.47	+0.24	−1.44	—	interface
TS_{18}	$*H^{\ddagger}H_2CO + *OH$	R_{05}	—	—	−1.21	+0.53	−1.32	+0.28	−1.11	+0.68	ZrO_2
R_{09}	$*H_3CO + *OH$	R_{05}	−2.50	−1.13	−2.71	−0.97	−2.64	−1.04	−2.73	−0.95	ZrO_2
R_{10}	$*H_3CO + *OH + 2\cdot *H$	R_{09}	−2.77	−0.27	−2.79	−0.08	−2.75	−0.10	−2.60	+0.13	ZrO_2
TS_{19}	$*H_3COH^{\ddagger} + *OH + *H$	R_{10}	—	—	−2.71	+0.08	−2.67	+0.08	−2.49	+0.10	ZrO_2
TS_{20}	$*H^{\ddagger}H_2COH + *OH + *H$	R_{08}	—	—	−0.27	+1.13	−1.07	+0.65	—	—	interface
R_{11}	$*H_3COH + *OH + *H$	R_{10}	−2.75	−0.49	−2.74	−0.34	−2.73	+0.02	−2.54	+0.06	ZrO_2
—	$H_3COH\,(g) + H_2O\,(g)$	R_{11}	−0.53	+2.22	−0.53	+2.21	−0.53	+2.20	−0.50	+2.05	—
TS_{21}	$*H_3C + OH^{\ddagger} + *OH + *H$	R_{11}	—	—	—	—	−1.29	+1.43	—	—	interface
I_{03}	$*H_3C + OH + *OH + *H$	R_{11}	−2.49	+0.26	−2.52	+0.22	−3.23	−0.51	—	—	interface
TS_{22}	$*CO + O^{\ddagger}$	I_{01}	—	—	—	—	+0.97	+1.73	—	—	interface
I_{04}	$*CO + *O$	I_{01}	—	—	+0.10	+1.27	−0.33	+0.43	—	—	interface

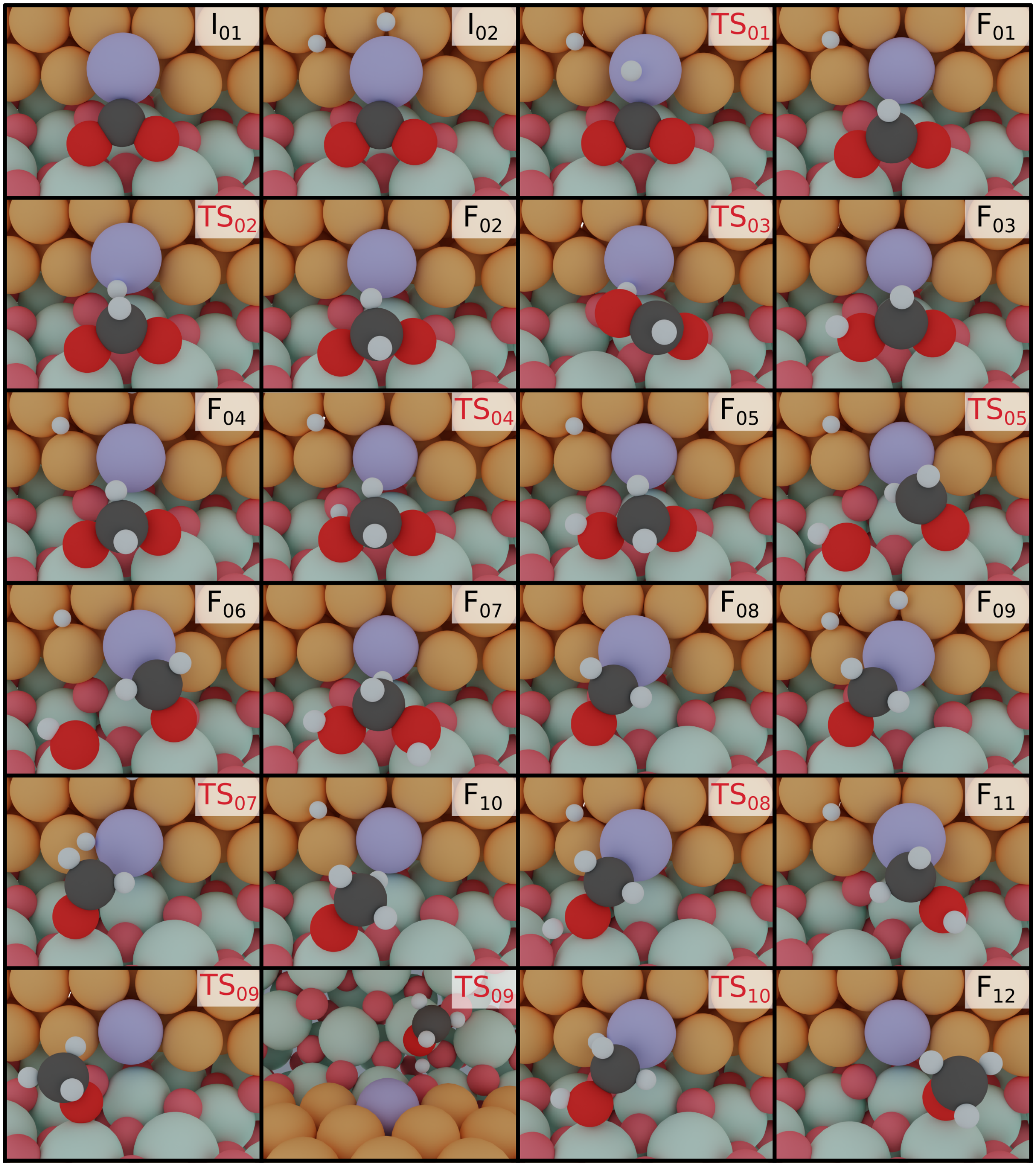

Figure S8: Adsorption at the Zn-dilute interface, the formate pathway. Light red: lattice O, dark red: adsorbate O, white: H, dark grey: C, purple: Zn, turquoise: Zr, orange: Cu.

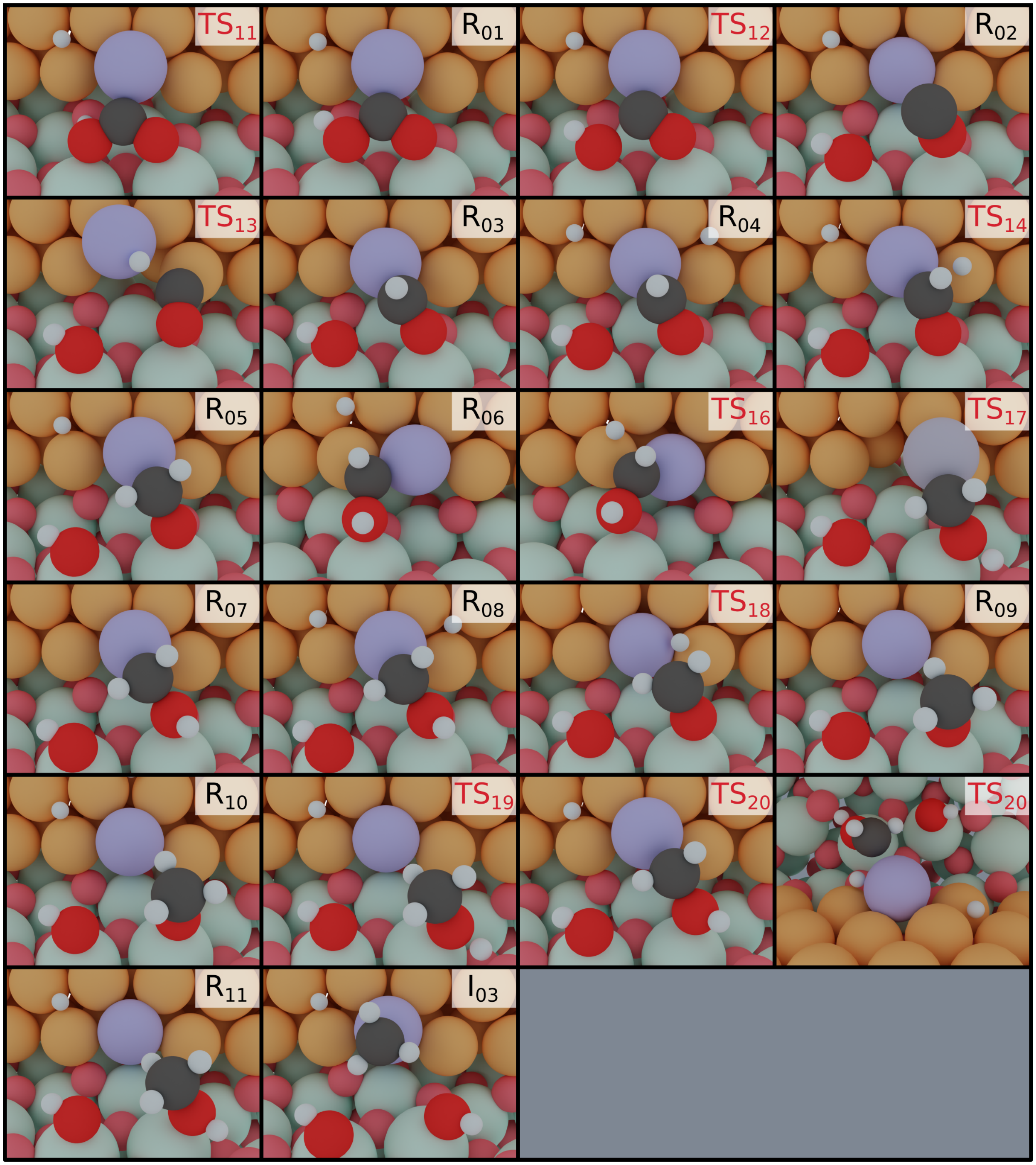

Figure S9: Adsorption at the Zn-dilute interface, the RWGS route. Light red: lattice O, dark red: adsorbate O, white: H, dark grey: C, purple: Zn, turquoise: Zr, orange: Cu.

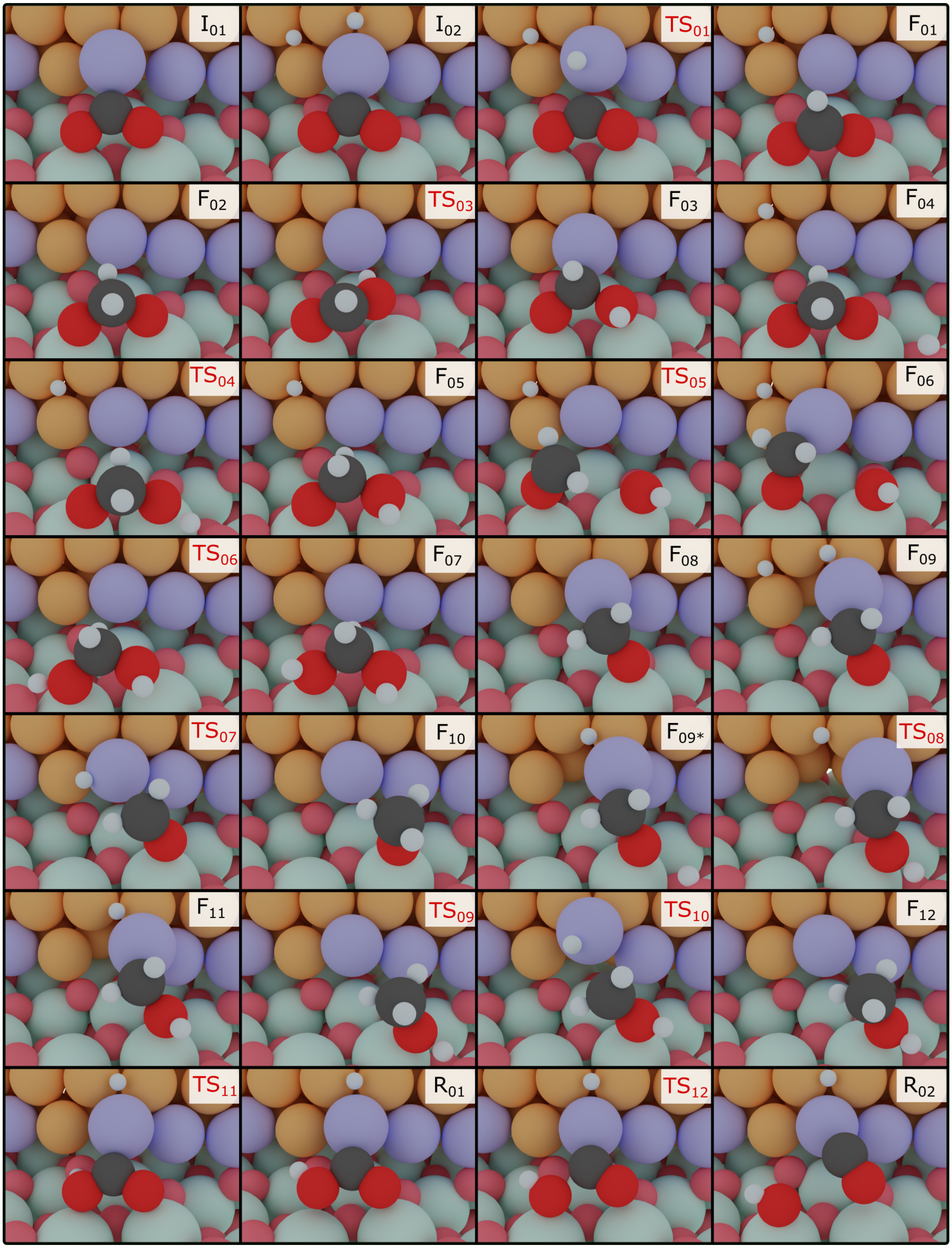

Figure S10: Adsorption at the Zn-rich interface, the formate pathway. Light red: lattice O, dark red: adsorbate O, white: H, dark grey: C, purple: Zn, turquoise: Zr, orange: Cu.

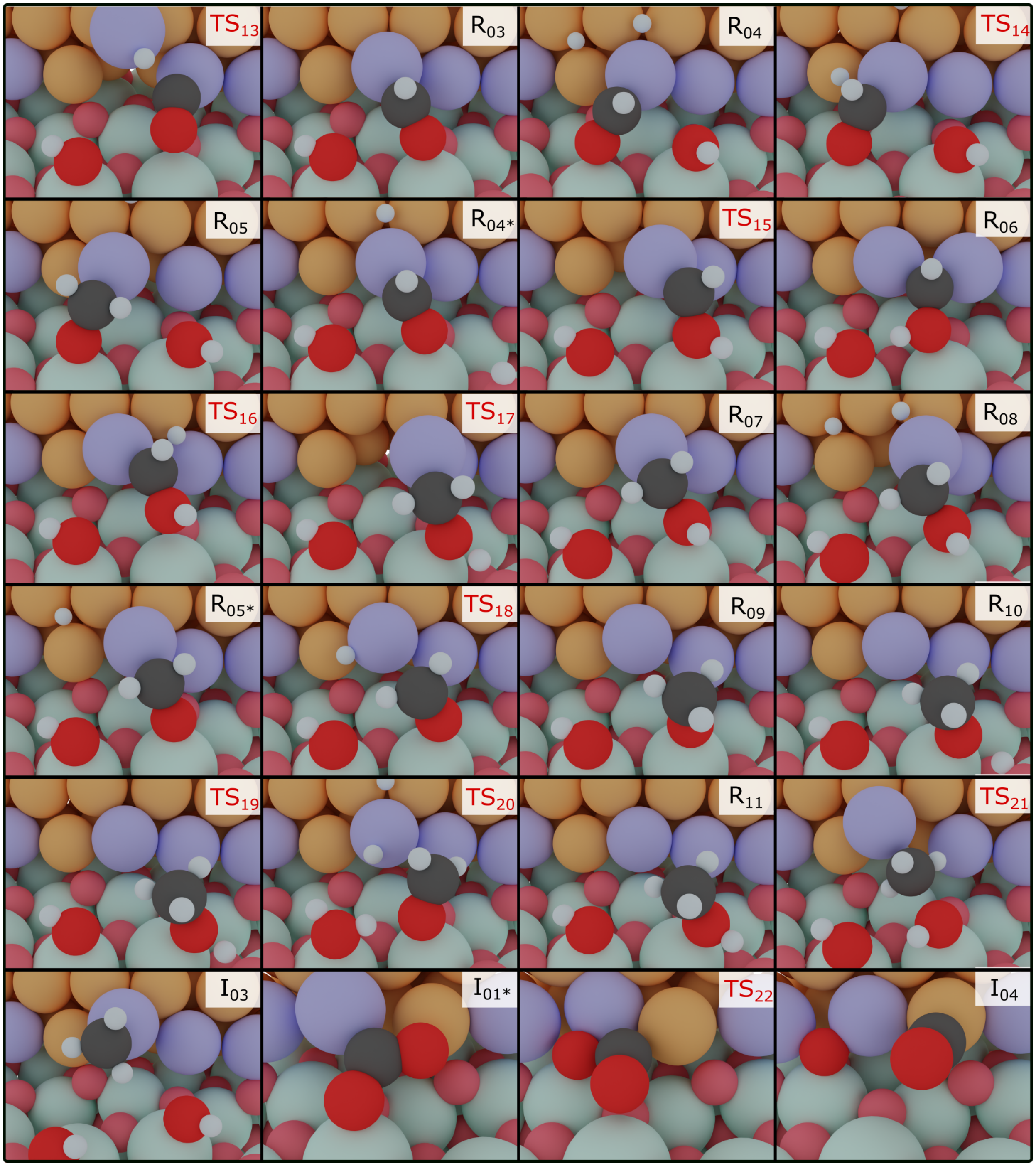

Figure S11: Adsorption at the Zn-rich interface, the RWGS route. Light red: lattice O, dark red: adsorbate O, white: H, dark grey: C, purple: Zn, turquoise: Zr, orange: Cu.

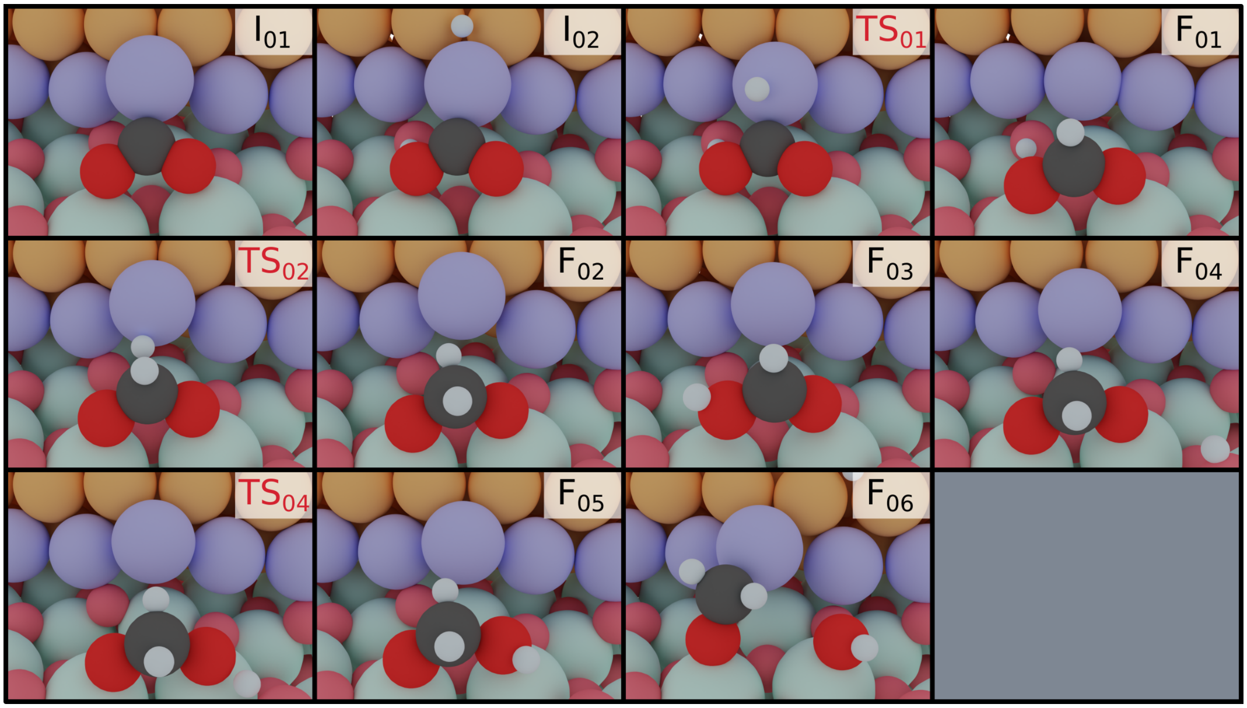

Figure S12: Adsorption at the Zn interface, the formate pathway. Light red: lattice O, dark red: adsorbate O, white: H, dark grey: C, purple: Zn, turquoise: Zr, orange: Cu.

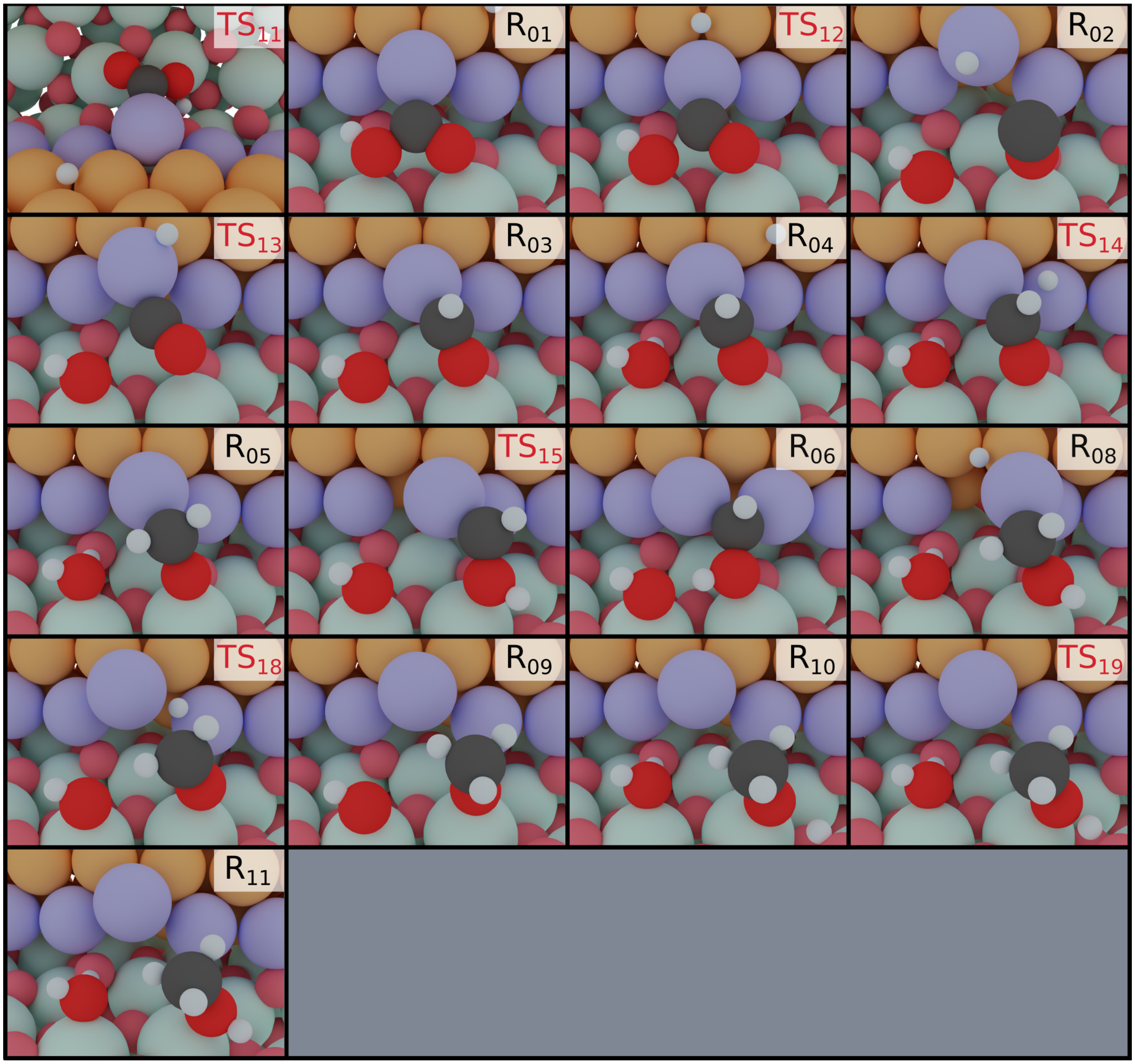

Figure S13: Adsorption at the Zn interface, the RWGS route. Light red: lattice O, dark red: adsorbate O, white: H, dark grey: C, purple: Zn, turquoise: Zr, orange: Cu.

3 Energetic span analysis

Degrees of turnover frequency control for each intermediate (I_j) and transition state (T_i) were calculated using equations (1) and (2).

$$X_{\mathrm{TOF},T_i,n} = \frac{\sum_j e^{(T_i - I_j + \delta G_{i,j})/RT}}{\sum_{i \in cycle_n, j} e^{(T_i - I_j + \delta G_{i,j})/RT}} \tag{1}$$

$$X_{\mathrm{TOF},I_j,n} = \frac{\sum_{i \in cycle_n} e^{(T_i - I_j + \delta G_{i,j})/RT}}{\sum_{i \in cycle_n, j} e^{(T_i - I_j - \delta G_{i,j})/RT}} \tag{2}$$

where again

$$\delta G_{i,j} = \begin{cases} 0 & \text{if } i \geq j \text{, TS follows intermediate} \\ \Delta G_r & \text{if } i < j \text{, TS precedes intermediate} \end{cases} \tag{3}$$

These equations can be derived from those originally defined by Kozuch and Shaik[7] by substituting $\delta G'_{i,j} = -\delta G_{i,j} + \Delta G_r$ and dividing both the numerator and the denominator by $e^{\Delta G_r/RT}$. In the terminology of the graph-based implementation, every intermediate (node) is included in each mechanism n, including intermediates that are not part of the most direct closed catalytic cycle. All nodes in the branches created are treated as belonging to the position of the branching-off point when determining the order of the states. Transition states (edges) in branches are ignored and the intermediates are assumed to be in a fast equilibrium. This allows us to calculate the exponential terms in equations 1 and 2 for each pairing of intermediate and main-cycle transition state separately for each mechanism. The final results are given as a weighted sum using the turnover frequencies determined for each mechanism despite the X_{TOF} values determined here being quite consistent between mechanisms with the same main cycle.

Some changes were made to the Python code written by Garay-Ruiz[8] (`https://gitlab.com/dgarayr/gtoffee`). Using NumPy arrays instead of matrices (which are officially deprecated) allows better use of NumPy's optimised code. After checking that the list

Table S3: Degrees of turnover frequency control (X_{TOF}) calculated for the Zn-dilute interface. The values are a weighted average of the X_{TOF} values in each mechanism belonging to the cycle. Only values greater than 0.001 are shown

	Cycle 1	Cycle 2	Cycle 3	Cycle 4
Intermediate				
HCOO+H	1.000	1.000	1.000	0.999
Transition state				
$H_2COH+H - H_3COH$	1.000	—	1.000	—
$H_2CO+2\,H - H_3CO+H$	—	1.000	—	0.685
$CO_2+2\,H - HCOO+H$	—	—	—	0.315

"mech_mat_list" is not empty, the for loop in the list comprehension can be changed to a much faster NumPy broadcasting operation. The modified and original codes were subjected to several runs and the changes outlined here did not affect any of the results.

From line 370 in nx_reaxgraf.py:

```
mech_mat = nx.to_numpy_matrix(mech_trial)
isomorph_check = [(mech_mat==mat).all() for mat in mech_mat_list]
isomorph_flag = np.any(isomorph_check)
```

was changed to

```
mech_mat = nx.to_numpy_array(mech_trial)
if len(mech_mat_list) != 0:
    ic_tmp = mech_mat == mech_mat_list
    isomorph_check = np.all(ic_tmp,(1,2))
    isomorph_flag = np.any(isomorph_check)
else: isomorph_flag = False
```

Similar changes were made from line 556 onward:

```
    tree_matrix = nx.to_numpy_matrix(tree_test,nodelist=main_nodelist)
        mat_check = [(tree_matrix == mat).all() for mat in tree_mat_list]
        isomorph_flag = np.any(mat_check)
```

was changed to

```
    tree_matrix = nx.to_numpy_array(tree_test,nodelist=main_nodelist)
    if (len(tree_mat_list) != 0):
        mc_tmp = tree_mat_list == tree_matrix
        mat_check = np.all(mc_tmp,(1,2))
        isomorph_flag = np.any(mat_check)
    else:
        isomorph_flag = False
```

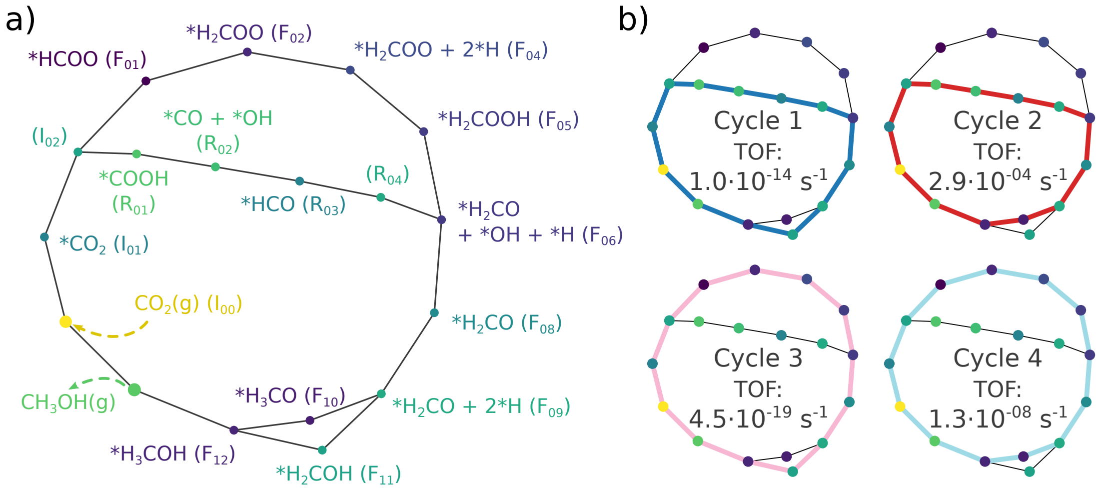

Figure S14: a) The simplified network used in the energetic span analysis. b) The catalytic cycles in the simplified network with their corresponding turnover frequencies on the Zn-rich interface.

References (Supporting Information)

(1) L. C. Grabow, M. Mavrikakis, *ACS Catal.* 2011, **1**, 365–384.

(2) M. Behrens, F. Studt, I. Kasatkin, S. Kühl, M. Hävecker, F. Abild-Pedersen, S. Zander, F. Girgsdies, P. Kurr, B.-L. Kniep, M. Tovar, R. W. Fischer, J. K. Nørskov, R. Schlögl, *Science* 2012, **336**, 893–897.

(3) S. Kattel, B. Yan, Y. Yang, J. G. Chen, P. Liu, *J. Am. Chem. Soc.* 2016, **138**, 12440–12450.

(4) S. Kattel, P. J. Ramírez, J. G. Chen, J. A. Rodriguez, P. Liu, *Science* 2017, **355**, 1296–1299.

(5) S. Kattel, P. Liu, J. G. Chen, *J. Am. Chem. Soc.* 2017, **139**, 9739–9754

(6) A. Arandia, J. Yim, H. Warraich, E. Leppäkangas, R. Bes, A. Lempelto, L. Gell, H. Jiang, K. Meinander, T. Viinikainen, S. Huotari, K. Honkala, R. L. Puurunen, *Appl. Catal. B: Environ.* 2023, **321**, 122046.

(7) S. Kozuch, S. Shaik, *Acc. Chem. Res.* 2011, **44**, 101–110.

(8) D. Garay-Ruiz, C. Bo, *ACS Catal.* 2020, **10**, 12627–12635.